PROCEEDINGS, 50th Workshop on Geothermal Reservoir Engineering
Stanford University, Stanford, California, February 10-12, 2025
SGP-TR-229

Mathematical Modeling of Preformed Particle Gel Transport in Fractured Geothermal Reservoirs

Philip H. Winterfeld[1], Baojun Bai[2], and Yu-Shu Wu[1]

[1]Colorado School of Mines, Golden CO, USA

pwinterf@mines.edu

ywu@mines.edu

[2]Missouri University of Science and Technology, Rolla, MO, USA

baib@mst.edu

Keywords: Preformed particle gels, mathematical modeling, geothermal reservoirs

ABSTRACT

We are developing swellable Preformed Particle Gels (PPG), which can control preferential fluid and heat flow through fracture networks to increase the performance of EGS reservoirs. Part of this development is a mathematical model and numerical simulator to simulate PPG treatments by considering coupled thermal-hydraulic-mechanical effects, and gel swelling kinetics and plugging efficiency, from which an optimized gel treatment design and operation can be achieved.

The starting point for our mathematical model is the TOUGH2-CSM formulation and code. The TOUGH2-CSM fluid and heat flow formulation is based on the TOUGH2 one for multiphase, multi-component, and multi-porosity systems, with the latter including the MINC and EDFM models. We modified our formulation to simulate injection of PPG into fractures. We developed an equation of state module for gel-water systems based on a previous TOUGH2 module that handles air and water since PPGs consist mostly of water. We use experimental studies of PPG flow through fractures to obtain the PPG flow formulation, formulating PPG flow as that of a shear-thinning fluid with a yield stress (Herschel-Bulkley fluid). Injected PPG consists of polymer-based particles that are swollen with water. When injected into a fracture whose walls are permeable, it was found that water leaks off through the fracture walls and a more concentrated PPG is deposited there as a filter cake. In addition, the transverse pressure gradient under which PPG flows can dehydrate the PPG, resulting in a more concentrated, flowing PPG and a separate flowing water phase. These features of PPG were also incorporated into our model, as well as the ability of PPG to swell over time.

Our simulator's features were verified by matching data from experimental studies. They include PPG injection into open fractures, which were used to verify our PPG rheology and longitudinal dehydration models, and PPG injection into a closed fracture, which were used to verify our transverse dehydration model. Finally, we applied our model to a synthetic EGS to ascertain the effect of blocking highly conductive fractures with PPG on energy production.

1. INTRODUCTION

Geothermal energy, which is thermal energy stored in the earth, is considered to be a green and renewable energy source. Energy is transferred through the earth from the solid inner and liquid outer core, at temperatures ranging from 4500 to 6000°C, through the mantle and to the crust, and that heat flow is augmented by energy production from radioactive decay of elements in the earth's mantle and crust. The total energy contained in the first 30 km of crust has been estimated to be of the order 10^{28} J (Lund, 2007), and with world energy production estimated to be of the order 10^{19} J in 2019 (IEA, 2021), it can be concluded that geothermal energy could last indefinitely.

There are two general categories of geothermal energy exploitation, hydrothermal geothermal systems and enhanced geothermal systems (EGS). In the former, underground reservoirs of hot water or steam are brought to the surface and the energy in the fluid is used for heating or electrical production. Hydrothermal geothermal systems are practical only where there is sufficient underground fluid and rock permeability. EGS can access the more abundant geothermal energy that lacks sufficient underground fluid and rock permeability, residing in what is referred to as hot dry rocks. An injection well is drilled into the rock and the region around the well is stimulated to create new fractures or open existing ones. This allows injected fluid to flow through the stimulated region and be heated, with the fluid being produced through a production well.

Heat production from an EGS depends on the hydraulic properties of the fracture network, which determine heat transfer from the heated rock to fluid flowing through the fracture network. One impediment to optimizing EGS performance is the short circuiting of flow through the network, where flow preferentially occurs through a high conductivity path, depleting the thermal energy of rock in the vicinity of that path but leaving the thermal energy of large volumes of rock elsewhere little changed. The ability to control flow fluid flow through the fracture network would be necessary in order to optimize EGS performance.

In the petroleum industry, wells are drilled into permeable rock formations in order to produce the in situ oil. Water is produced as well and excess water production, often from high permeability zones, is undesirable and has been mitigated by the use of diverting agents that selectively plug these high permeability zones and decrease water production. One type of diverting agent is preformed particle gels (PPGs) (Bai et al., 2007a; Bai et al., 2007b). These gels are synthesized in surface facilities using an acrylamide monomer and a cross linker and then dried, ground into particles, and sieved in order to have a uniform particle size. Water is added to the uniform PPG particles, which causes them to swell and then they are injected into the formation, extruding through fractures and channels and blocking flow of subsequently injected fluid through them.

We are developing PPGs that can be used under conditions commonly encountered in EGS. These PPGs must be stable from 150 to 275 °C for more than six months, capable of being delivered into large aperture fractures, and able to plug those fractures very efficiently. Part of this work is to develop a model of PPG transport in EGS reservoirs. Previous attempts at developing related models include Charoenwongsa et al. (2012), who modeled gel flow in fractures during hydraulic fracturing and included non-Newtonian flow and filter cake formation in their model, and Goudarzi et al. (2013) who presented a simulator called UTGEL which can be used for modeling PPG transport through porous and fractured media that included permeability reduction due to PPG swelling and a PPG rheology model. In this work, we present a mathematical model, validated by lab results, of PPG transport in fractured EGS reservoirs.

2. TOUGH2-CSM DESCRIPTION

The starting point for our simulator is our TOUGH2-CSM thermal-hydrological-mechanical model. The TOUGH2-CSM fluid and heat flow formulation is based on the TOUGH2-MP formulation (Pruess et al., 1999; Zhang et al., 2008) of mass and energy conservation equations that govern fluid and heat flow in general multiphase, multicomponent, multi-porosity systems. The TOUGH2-CSM geomechanical formulation, added later, is based on the linear theory of elasticity for multi-porosity, non-isothermal media (Winterfeld and Wu, 2014; Winterfeld and Wu, 2016). The governing partial differential equations for mass balances and geomechanics are solved using the integral finite difference (IFD) numerical method (Narasimhan and Witherspoon, 1976; Pruess et al., 1999) for the spatial discretization. The time is discretized using a first order finite difference approximation. The final discrete non-linear equations are solved using a Newton iteration scheme. The IFD approach has proven to be computationally efficient in modeling highly non-linear three-phase flow problems and at the same time it has flexibility in handling complicated geometry or irregularity of a reservoir domain.

TOUGH2-CSM provides a general approach to modeling flow through fractured/porous systems using a generalized dual-continuum approach, such as the double-porosity (Warren and Root, 1963), the dual-permeability, the multiple porosity (Wu and Pruess, 1988), and the MINC (Pruess and Narasimhan, 1985) approaches, as developed and applied in the TOUGH2 code (Pruess et al., 1999). Besides the generalized dual-continuum approach, we have also modeled discrete fractures using the Embedded Discrete Fracture Method (EDFM) (Winterfeld et al., 2019) where fractures are approximated as rectangular regions that represent the fracture area, and an associated fracture aperture. Fracture properties, such as permeability and aperture, can be correlated to stress, pressure, and temperature.

3. MODIFICATIONS FOR PPG TRANSPORT

3.1 EOS module

We use an equation of state (EOS) module for fluid property calculation, namely density, viscosity, and enthalpy. The starting point for this module is the TOUGH2 EOS3 module (Pruess et al., 1999), which has aqueous and gaseous phases and two components, the first being water and the second being air. We generalized EOS3 to n components, with the gel component as the third component, the aqueous portion of gel phase the fourth, plus any others such as ions. There are also additional gel phases (one or two) that are composed of components three and higher.

PPG absorbs water and can swell up to 200 times its size (Bai et al., 2007a). Swollen PPG is mostly water so we assume the molar densities of aqueous (*aq*) and PPG (*gel*) phases are equal:

$$\rho_{gel} = \frac{\rho_{aq}}{M_{w,1}\sum_j \frac{X_{gel,j}}{M_{w,j}}} \tag{1}$$

where $M_{w,k}$ is component k molecular weight, $X_{p,k}$ is component k mass fraction in phase p. Aqueous phase density is calculated by EOS3 and depends on pressure and temperature.

3.2 PPG Fracture Flow

Zhang and Bai (2010) injected PPG into a fracture model consisting of two acrylic plates separated by a small distance. They correlated pressure drop and flow rate as:

$$\Delta P = Aq^B \tag{2}$$

where A and B are parameters. Seright (2001) observed during experiments of gel flow through fractures that gel would extrude through the fracture once a minimum pressure gradient, ∇P_{min}, is reached and correlated this pressure gradient with fracture aperture:

$$\nabla P_{min} \sim \frac{1}{h^2} \tag{3}$$

where h is fracture aperture. The proportionality constant implied by Equation 3 was obtained for a specific gel at specific conditions.

We conceptualize fractures as narrow slits and Equations 2 and 3 suggest flow of a shear-thinning fluid with a yield stress, the Herschel-Bulkley (HB) fluid, through a narrow slit. The relationship between flow rate and pressure gradient for steady-state flow of a HB fluid through a thin slit is:

$$q = \begin{cases} Hh^3 \frac{\left(\frac{h}{2}\right)^{\frac{1}{n}-1}}{4\left(\frac{1}{n}+2\right)}\left(1-\frac{2z_0}{h}\right)^{\frac{1}{n}+1}\left(1+\frac{2z_0}{\left(\frac{1}{n}+1\right)h}\right)\left(-\frac{\nabla P}{K}\right)^{\frac{1}{n}}; & \frac{2z_0}{h} < 1 \\ 0; & \frac{2z_0}{h} \geq 1 \end{cases} \tag{4}$$

and

$$z_0 = -\frac{\tau_0}{\nabla P} \tag{5}$$

where H is fracture height, K is power-law coefficient, n is power-law exponent, and τ_0 is yield stress. If we know the proportionality constant in Equation 3 for the fluid, we could estimate the yield stress assuming that fluid flow would start at the minimum pressure gradient:

$$\tau_0 = -h\frac{\nabla P_{min}}{2} \tag{6}$$

In addition, Equations 3 and 6 allows yield stress to be scaled to different fracture apertures.

In TOUGH2-CSM, fluid flow is governed by Darcy's law. For flow of PPG, we replace Darcy's law with Equation 4.

3.3 PPG Longitudinal Dehydration

Bai (2023) injected PPG into fractures with impermeable walls. Fluid leaving the fracture outlet was monitored, with aqueous phase flowing for a time followed by gel phase. It was observed that the volume of PPG needed to fill the fracture, defined when PPG would first be produced at the fracture outlet, was significantly greater than the fracture volume indicating that flowing PPG undergoes dehydration longitudinally.

Figure 1 is a schematic from the Lagrangian perspective of a fluid element, consisting of gel and aqueous phases, flowing through space from a pressure gradient imposed on it. This pressure gradient, an unbalanced force that acts on the fluid element, also causes the gel phase portion to dehydrate. As we follow the fluid element through space, the gel phase shrinks and the aqueous phase grows. Because gel and aqueous phases have different rheology, they would move at different velocities for a given pressure gradient and this is included in Figure 1 by the distortion of the fluid elements. As PPG dehydrates, its gel component mass fraction increases and a flowing aqueous phase is generated. We express longitudinal gel phase dehydration as the change in gel component mass fraction of the fluid element with time and assume it is

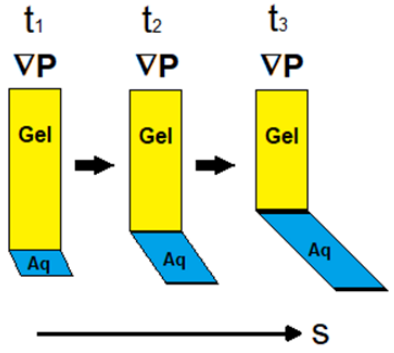

Figure 1: Fluid element, consisting of gel and aqueous phases, flowing through space. Fluid element shape distorts due to differing rheology between phases.

proportional to the pressure gradient acting on the fluid element. We then note that time and spatial position (coordinate S) are related by the gel velocity, v_{gel}:

$$\frac{dX_{gel,gel}}{dt} = \frac{dX_{gel,gel}}{dS}\frac{dS}{dt} = \frac{dX_{gel,gel}}{dS} v_{gel} = C_{dhyd}\nabla P \tag{7}$$

where C_{dhyd} is the dehydration coefficient.

In our finite difference formulation, fluid flows from one grid block to an adjacent one, shown in

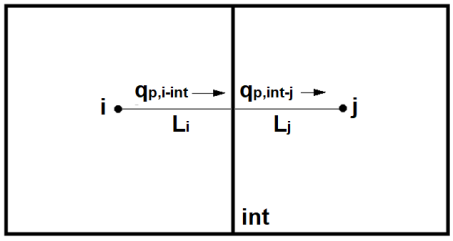

Figure 2: Adjacent grid blocks *i* and *j* with interface (*int*) and phase flows leaving grid block *i* and entering grid block *j*.

Figure 2, where the flow direction is from grid block *i* to *j*. The flow of a conserved component leaving grid block *i*, denoted by *i-int*, is the same as that entering grid block *j*, denoted by *int-j*. We apply this to flow of gel phase from grid block *i* to *j* with longitudinal dehydration. Gel phase leaving grid block *i* enters grid block *j* as gel phase that has incrementally dehydrated plus some additionally flowing aqueous phase. Conservation of mass equations for the gel component and those in aqueous phase are:

$$q_{gel,i-int}X_{gel,gel,i-int} = q_{gel,int-j}X_{gel,gel,int-j} \tag{8}$$

$$q_{gel,i-int}X_{gel,k,i-int} = q_{gel,int-j}X_{gel,k,int-j} + \Delta q_{aq,int-j}X_{aq,k,int} \tag{9}$$

where k refers to aqueous phase components and Δq_{aq} is the additional aqueous phase generated by longitudinal dehydration. Mass fractions subscripted *i-int* in Equations 8 and 9 are evaluated at grid block *i* and the gel phase flow rate is the finite difference version of Equation 4 for flow between two grid blocks. We integrate Equation 7 from grid block *i* to the interface (*int*) to obtain the gel component mass fraction of gel phase entering grid block *j*:

$$X_{gel,gel,int-j} = X_{gel,gel,i-int} + \frac{C_{dehy}}{v_{gel}} L_i \nabla P \tag{10}$$

The remaining unknowns on the right hand side of Equations 8 and 9 can then be solved for in terms of grid block i quantities.

3.4 PPG Transverse Dehydration

PPG can also dehydrate transversely when flowing through fractures with permeable walls, forming a filter cake on the fracture wall. Wang and Bai (2018) injected PPG into cylindrical

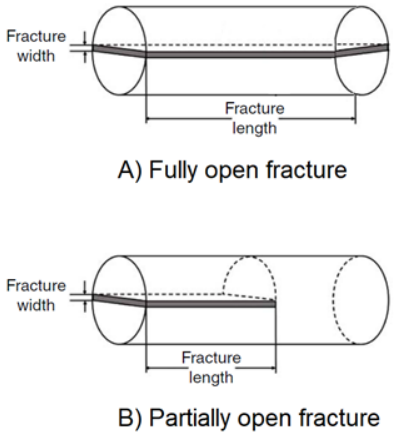

Figure 3: Schematic of fully (A) and partially (B) open fractures used in Wang and Bai (2018) experiments.

Berea sandstone cores that had fully and partially open fractures, as shown in Figure 3. In these experiments, injected PPG accumulated and dehydrated at the fracture walls and tip, forming a filter cake that consisted of concentrated gel particles, with the aqueous portion of the PPG leaking off through the fracture walls. Seright (2003) also observed filter cake formation during gel flow through fractures and presented two models of filter cake formation, one being the well-known Carter model (Howard and Fast, 1957) as well as proposing an alternative one. We include both of these formulations in our model.

3.4.1 Carter Model

Figure 4 shows a fracture with filter cake on the wall, flowing PPG to the right of the filter cake,

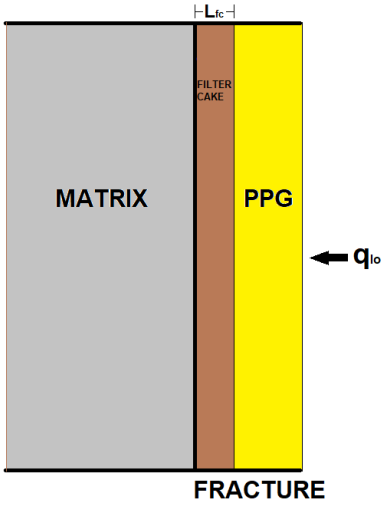

Figure 4: Schematic of fracture-matrix interface with filter cake on the fracture wall, flowing PPG in the fracture, and leak off of aqueous phase to the matrix.

and matrix to the left. The pressure drop between the fracture and the matrix causes flow between the two. The polymer portion (gel component) of PPG cannot flow into the matrix so it is deposited at the base of the filter cake, causing the filter cake to grow. This is accompanied by release of aqueous fluid from the PPG (dehydration) that flows through the filter cake and into the matrix.

A mass balance for gel component relates the growth of the filter cake to the leaking off rate:

$$q_{lo}\rho_{gel}S_{gel}X_{gel,gel} = \left(\rho_{fc}S_{fc}X_{fc,gel} - \rho_{gel}S_{gel}X_{gel}\right)\frac{\partial L_{fc}}{\partial t} \tag{11}$$

where q_{lo} is overall leaking off rate, subscript $_{fc}$ refers to filter cake, and L_{fc} is filter cake thickness. The filter cake is assumed incompressible and has a constant composition with a gel component mass fraction greater than that of flowing gel phase. If filter cake consists only of dehydrated gel phase, filter cake saturation (S_{fc}) would be one. Filter cake is permeable to aqueous phase (Seright 2003) and an overall mass balance on gel and aqueous components would show the leaking off rate of aqueous fluid entering the matrix equals the gel phase leaking off rate.

3.4.2 Seright Model

The Carter model is a highly idealized model of filter cake formation in that it assumes filter cake grows uniformly on the fracture wall. Seright (2003) proposed an alternative model. They injected gel into an open fracture with permeable walls and observed that produced gel was very similar in composition to injected gel. In addition, there was aqueous phase leaving the fracture and formation of immobile concentrated gel (filter cake) that contacted the fracture wall. Injected gel wormholed through concentrated gel and contacted the fracture wall as well. Aqueous phase leaving the fracture from these wormholes was greater than that through the immobile gel. As more gel was injected, the amount of immobile gel increased and less fracture wall area was contacted by the mobile gel wormholes.

In this model, mobile gel dehydrates to form a concentrated immobile gel phase. The fracture surface area is contacted by either mobile or immobile gel (as well as aqueous phase) and the area covered by immobile gel depends on gel concentration where:

$$A_{im} + A_{mo} + A_{aq} = 1 \tag{12}$$

$$A_{im} = (1 - A_{aq})A_{im}\left(\frac{C_0}{C}\right) = (1 - A_{aq})\frac{\frac{C}{C_0} - 1}{\frac{C}{C_0}} \tag{13}$$

where A is fractional fracture wall area, subscript *im* refers to immobile gel, subscript *mo* refers to mobile gel, C is gel concentration (gel mass per unit volume), and subscript *0* refers to injected gel. Figure 5 shows a schematic of mobile and immobile gel phases, and aqueous phase.

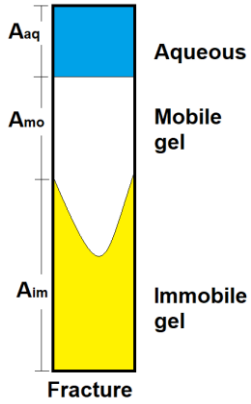

Figure 5: Fracture with mobile and immobile gel phases, and aqueous phase. The fracture wall area contacted by each phase is also shown.

The fracture wall area contacted by a gel phase can differ from its volume fraction.

The formation of immobile gel occurs in two steps. The first step is similar to filter cake formation in the Carter model. The aqueous portion of mobile gel leaks off into the matrix, leaving a volume of immobile gel:

$$q_{lo}A_{mo}\rho_{mo}S_{mo}X_{mo,gel} = \left(S_{fc}\rho_{im}X_{im,gel} - \left(S_{mo}\rho_{mo,gel}X_{mo,gel} + S_{im}\rho_{im}X_{im,gel}\right)\right)\frac{dW}{dt} \tag{14}$$

where W is the immobile gel volume. In the second step, the immobile gel saturation is updated by uniformly dispersing the above immobile gel volume into the rest of the fracture volume:

$$V\frac{dS_{im}}{dt} = (S_{fc} - S_{im})\frac{dW}{dt} \tag{15}$$

The immobile gel volume term is eliminated from Equations 14 and 15 to yield an equation for immobile gel phase saturation.

3.5 Gel Swelling Kinetics

PPG is formed from acrylamide polymer that can absorb water and swell. We incorporated this phenomenon into our model by adding PPG swelling kinetics. Experiments to determine PPG swelling ratio versus time (Bai, 2023b) are part of this work and an example is shown in Figure 6. Swelling ratio is defined as:

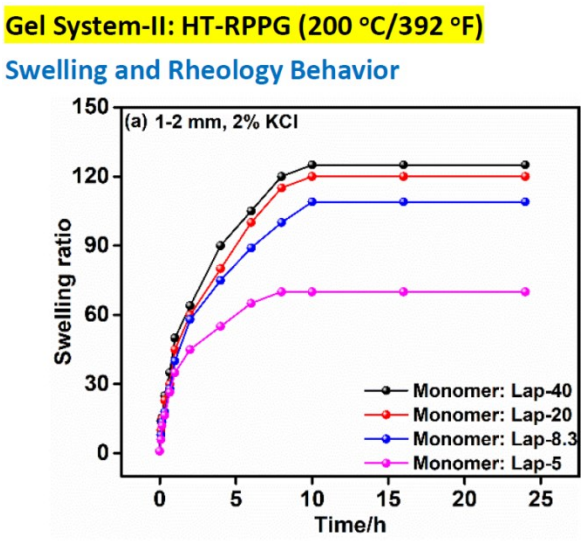

Figure 6: Experimentally determined PPG swelling ratio versus time.

$$S_R = \frac{w_{SG} - w_{DHG}}{w_{DHG}} \tag{16}$$

where w is weight, subscript SG refers to swollen gel, and subscript DHG refers to dehydrated gel. We chose the following function to fit the swelling ratio data:

$$S_R = S_{R,EQ}(1 - e^{-At}) \tag{17}$$

where subscript EQ refers to fully swollen gel and A is a parameter. The swelling ratio is related to gel component mass fraction:

$$X_{gel,gel} = \frac{w_{DHG}}{w_{SG}} = \frac{1}{S_R + 1} = \frac{1}{S_{R,EQ}(1 - e^{-At}) + 1} \tag{18}$$

Figure 7 shows a schematic of gel swelling. From time T_1 to a later time, T_2, the gel phase has swelled, resulting in a greater volume of gel phase and a smaller volume of aqueous phase. The gel and aqueous component mass balances are modified to

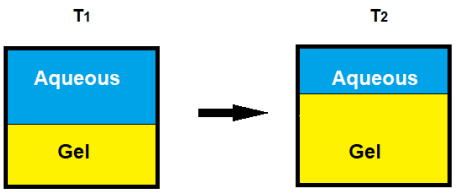

Figure 7: Schematic of gel swelling staring with gel and aqueous phases on the left at time T1 and those phases at a later time T2 where the gel phase has swelled, absorbing some of the aqueous phase.

account for gel swelling. The rate of gel phase swelling is the change in mass of aqueous components in the gel phase with respect to time. This mass ($m_{gel,aq}$) is given by:

$$m_{gel,aq} = \rho_{gel} S_{gel}(1 - X_{gel,gel}) \tag{19}$$

During gel phase swelling, the mass of gel component in gel phase remains constant. This mass is given by:

$$m_{gel,gel} = \rho_{gel} S_{gel} X_{gel,gel} \tag{20}$$

We differentiate Equation 19 with respect to time and with the constraint that Equation 20 is constant to obtain:

$$\left(\frac{\partial m_{gel,aq}}{\partial t}\right)_{m_{gel,gel}} = A\rho_{gel}S_{gel}X_{gel,gel}\left(1 + S_{R,EQ} - \frac{1}{X_{gel,gel}}\right) \quad (21)$$

Equation 21 is the rate of mass loss of aqueous components for the aqueous phase as well as mass gain of aqueous components for the gel phase.

4. EXAMPLE SIMULATIONS

4.1 Rheological Model Verification

In our first set of simulations, we verified our PPG rheological model by matching experiments done by Zhang and Bai (2010). In these experiments, PPG was swollen using brine of various concentration (0.05, 0.25, 1, and 10 weight percent) and injected into fractures consisting of two impermeable plates separated by a small distance (0.5, 1.0, and 1.5 mm) at various rates (5, 10, 15, 20, 25, and 30 ml/min). The plate areal dimensions were 55×10 cm. Our primary simulation grid, over the plate's areal dimensions, was uniform and 11×11. We used EDFM to add a fracture to the uniform grid. We injected PPG at one end of the grid and produced fluid from the other until steady-state was reached.

Equation 2 shows the Zhang and Bai (2010) correlation of injection pressure to injection rate. We used the exponent *B* as the power law exponent and varied the power law index of the HB fluid to match the injection pressure for the 5 ml/min injection rate. We then ran the other injection rates. The yield stress was zero. Figure 8 compares simulated and experimental injection pressure for the 0.25 weight

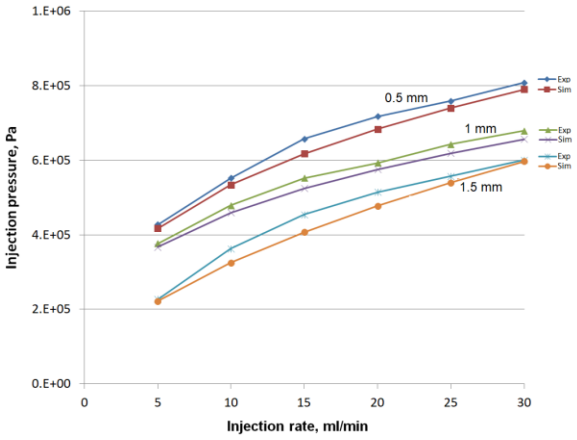

Figure 8: Simulated and experimental injection pressure for PPG swollen in 0.25 weight percent brine.

percent case. The matches at rates over 5 ml/min were good, indicating that the rheological model captures the dependence of pressure drop on flow rate for a given fracture aperture. We then ran cases with nonzero yield stress and an example for the 1 weight percent brine and 0.5 mm fracture aperture case is shown in Figure 9. Results for the zero yield stress case are also shown for comparison

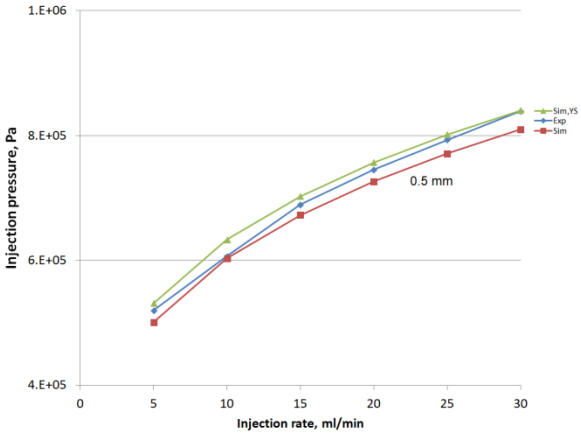

Figure 9: Simulated, with zero and non-zero yield stress, and experimental injection pressure for a 0.5 mm fracture with injected PPG swollen in 1 weight percent brine.

in the figure. The non-zero yield stress case translates the data upward and can improve the match over the zero yield stress case.

4.2 Longitudinal Dehydration Simulation

Bai (2023a) constructed fracture models from limestone cores by cutting them lengthwise into equal parts and reassembling the halves while keeping a small distance between them using spacers. In one set of experiments, the cores were coated with epoxy in order to make the matrix impermeable. PPG was injected into the fracture model at 1, 5, and 10 ml/min until the pressure stabilized. There was a minimum pressure required for the gel to enter the fracture, called the threshold pressure, and a pressure at which PPG is first produced, called the breakthrough pressure. The amount of PPG injected from the threshold pressure to the gel breakthrough pressure is the volume needed to fill the fracture, and was multiples of the fracture volume, indicating that longitudinal dehydration was taking place.

In our next set of simulations, we modeled one of these experiments. The fracture areal dimensions were 3.81×28 cm and the fracture aperture was 1 mm. The primary grid was 28×1 and we used EDFM to add a fracture to the uniform grid. We injected PPG into the fracture and produced fluid from the other end until PPG broke through there.

The swelling ratio of gel was 50 yielding a gel component mass fraction of 0.0196. Data from Zhang and Bai (2010) gave us a power law exponent of 0.311. In addition, gel dehydration can affect gel rheology, so we let power law index vary with gel component mass fraction and data in that reference suggested a slope of 2000 for this variation. We used the power law index and dehydration coefficient (which included the gel velocity term in Equation 10) as parameters to match the gel breakthrough pressure ($8.14 \cdot 10^5$ Pa) and completely fill the fracture with gel phase at that pressure. We obtained values of 790 and $1.2 \cdot 10^{-7}$, respectively, for this match.

Figure 10 shows gel component mass fraction versus distance along the fracture. Injected PPG underwent longitudinal dehydration as it flowed through the fracture so gel component mass

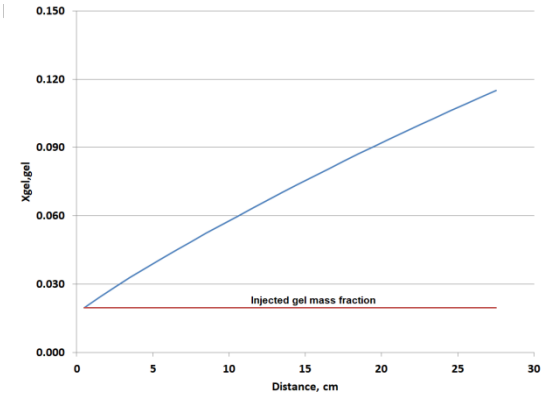

Figure 20: Gel component mass fraction versus distance along the fracture.

fraction increased with distance along it.

4.3 Transverse Dehydration Simulation

Wang and Bai (2018) constructed fracture models from Berea sandstone cores. One such model was a partially open fracture, made by cutting a core along its axis to half of its length, and reassembling the core with spacers to form a fracture, as shown in Figure 4B. PPG was injected into the fracture at 1 cm^3/min until the pressure reached 1000 psi (6.89 MPa) and water was injected at that rate afterwards. During PPG injection, aqueous phase was continuously produced from the fracture end after flowing through the permeable core. The total volume of PPG injected was much greater than the fracture volume and observations of the cores showed the formation of filter cake inside the fracture.

We modeled this experiment. The core dimensions were 16×2.35 cm and the fracture aperture was 0.5 mm. The primary grid was 16×1 and we used EDFM to add a fracture that extended half of its length. Figure 11 shows the matrix and fracture grid blocks. The 16 matrix grid blocks

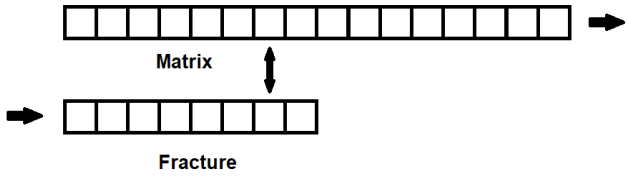

Figure 13: Grid for partially open fracture. The left half contains matrix and fracture grid blocks; the right half only matrix grid blocks. Horizontal arrows indicate injection (left) and production (right); the vertical arrow indicates matrix-fracture flow and applies to all fracture grid blocks.

span the core length, and the 8 fracture grid blocks span half of the core length. There is flow between each of the corresponding matrix and fracture grid blocks, indicated by the up and down arrow. The horizontal arrow on the left signifies injection into the fracture and that on the right signifies production (aqueous phase) from the core.

The core permeability was 50 md ($4.93 \cdot 10^{-14}$ m^2). PPG rheology was power law with index of 140 and exponent of 0.268. Gel component mass fraction was 0.03. During injection, gel phase forms a growing filter cake on the fracture wall with aqueous phase flowing through the filter cake and into the matrix. Parameters adjusted to match experimentally measured pressure were filter cake gel component mass fraction and filter cake permeability, 0.53 and $3.5 \cdot 10^{-19}$ m^2, respectively. Figure 12 compares measured and simulated pressures as a function of

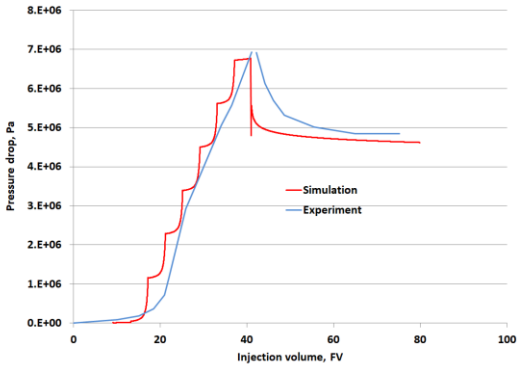

Figure 42: Measured and simulated pressures for partially open fracture.

injection volume whose units are fracture volumes (FV). The pressure buildups are similar, with the periodic oscillations in simulation being a consequence of using a finite difference formulation to simulate the system. Water injection began around 40 FV and the steady-state pressures afterwards are similar as well.

4.4 Fracture Plugging Model

We ran a simulation to demonstrate the ability of PPG to plug fractures. We considered two horizontal fractures in impermeable rock, with both intersecting a wellbore into which PPG is injected, as shown in Figure 13. The simulation domain was 20×10×75.2 m and was two-dimensional. The two fractures were spaced about 25 m apart. Fluid injected into the well bore, on the left side of the domain, would flow through the fractures and be produced to the surroundings at the right side of the domain. The arrows in the figure signify flow directions,

with injected fluid being able to transverse the length of the well bore and horizontal flow through each fracture to the surroundings. The rest of the domain is impermeable matrix.

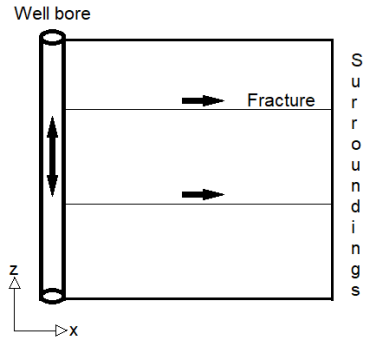

Figure 53: Schematic of the two-fracture simulation domain.

The simulation domain was discretized into a 20×1×5 primary grid. The primary grid is comprised of the five-block unit shown Figure 14.

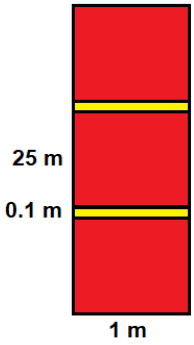

Figure 64: Five-block unit that comprises a column of the primary grid.

The x-direction dimension of all grid blocks is 1 m; the z-direction dimension of the yellow grid blocks is 0.1 m and that of red ones is 25 m. There are twenty of these columns. For columns other than the first, the yellow grid blocks contain matrix and fracture and the red grid blocks contain only matrix. The first column of grid blocks contains the well bore, which is modeled as a vertical fracture. The yellow grid blocks in that column contain matrix, fracture and the well bore, and the red grid blocks contain matrix and the well bore. Primary grids that contain only matrix are single porosity; the rest are double porosity with the fractures and well bore lumped into a single continuum.

The upper fracture in Figure 14 was highly conducting with permeability was set at 10^{-8} m^2, and the lower one had a fracture permeability was set at 10^{-11} m^2. In order to have negligible pressure gradients in the well bore, the well bore permeability was set to a high value, 10^{-7} m^2. PPG rheology (K, n, τ_0) was (300, 0.311, 1436). We first injected PPG at $6.12 \cdot 10^{-2}$ kg/s for 20,000 seconds. Afterwards, we injected water at the same rate. Figure 15 shows the

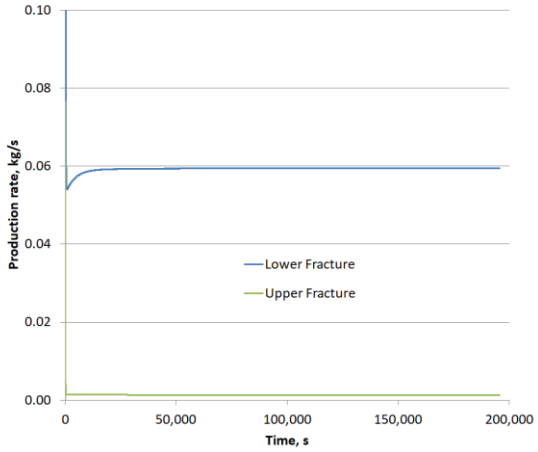

Figure 75: Production rate versus time for upper and lower fractures during water injection, which starts at time zero.

production rate at the right side of the grid (the surroundings) versus time for the upper and lower fractures, with time equals zero being at the beginning of water injection. Essentially all of the injected fluid was exiting the lower fracture. During PPG injection, PPG mostly entered the high permeability (upper) fracture. Afterwards, injected water only flowed into the low permeability (lower) fracture since the pressure gradient for water flow was not large enough to exceed the PPG yield stress and cause the PPG in the upper fracture to flow.

4.5 EGS Energy Production Simulation

Finally, we ran a simulation to demonstrate the effect plugging highly conductive fractures would have on energy production from an EGS. Based on data from the literature (Habanero, 2014), we constructed a synthetic EGS whose dimensions were 300×140×500.5 m and contained of five horizontal fractures spaced about 100 m apart. An injector was situated on the left side of the domain that communicated with the five horizontal fractures. Fluid injected into the injector would flow through the five fractures to the producer at the right side of the domain. Figure 16 shows a schematic of the simulation domain. Excluding the fractures, the rest of the domain is impermeable matrix.

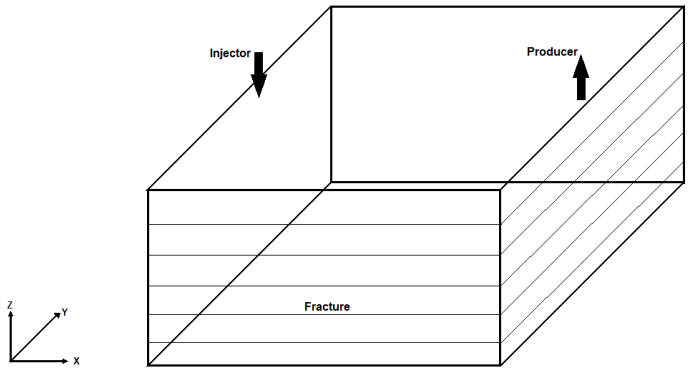

Figure 86: Schematic of the EGS simulation domain.

The simulation domain was discretized into a 15×7×25 primary grid. The primary grid is comprised of the five-block unit shown Figure 17.

Figure 97: Five-block unit that comprises the primary grid.

The x- and y-direction dimensions of all grid blocks are 20 m; the z-direction dimension of the yellow grid blocks is 0.1 m and that of red ones is 25 m. Each grid block column consists of five of these units stacked vertically, and there are 105 of these columns. For columns other than the one containing the injector, the yellow grid blocks contain matrix and fracture and the red grid blocks contain only matrix. The injector is modeled as a vertical fracture. In its column, the yellow grid blocks contain matrix, fracture and the injector, and the red grid blocks contain matrix and the injector. Primary grids that contain only matrix are single porosity; the rest are double porosity with the fractures and injector lumped into a single continuum. The producer is a constant pressure sink.

In our EGS, the middle fracture in Figure 16 was highly conducting with an aperture of 1 cm, and the rest were less conducting with an aperture of 1 mm. The former fracture permeability was set at 10^{-10} m^2; we assume fracture permeability is proportional to aperture squared, so the latter ones were set to 10^{-12} m^2. In order to have negligible pressure gradients in the injector, its permeability was set to a high value, 10^{-7} m^2. The initial temperature of the EGS was 275 °C, the initial pressure was 71.5 MPa, and we injected 50 °C water at 0.5 kg/s.

We first simulated ten years of water injection; temperature profiles are shown in Figure 18. The profile on the left is the xz-cross section,

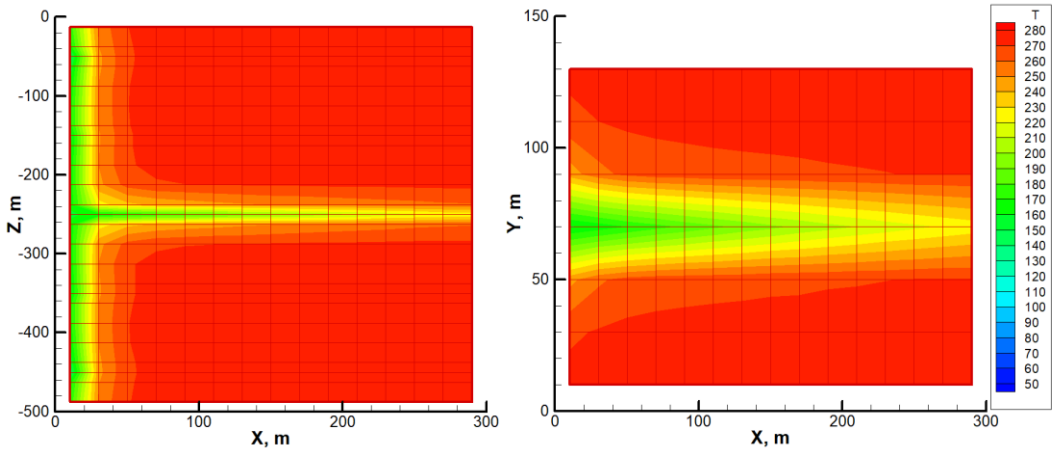

Figure 108: Temperature profiles in EGS after ten years of water injection.

which passes through the injector. The profile on the right is the xy-cross section that passes through the middle, high permeability fracture. Injected water flows through that fracture almost exclusively. We continued water injection until twenty years and the temperature profiles are shown in Figure 19. The profiles are similar with the cooler regions expanding somewhat.

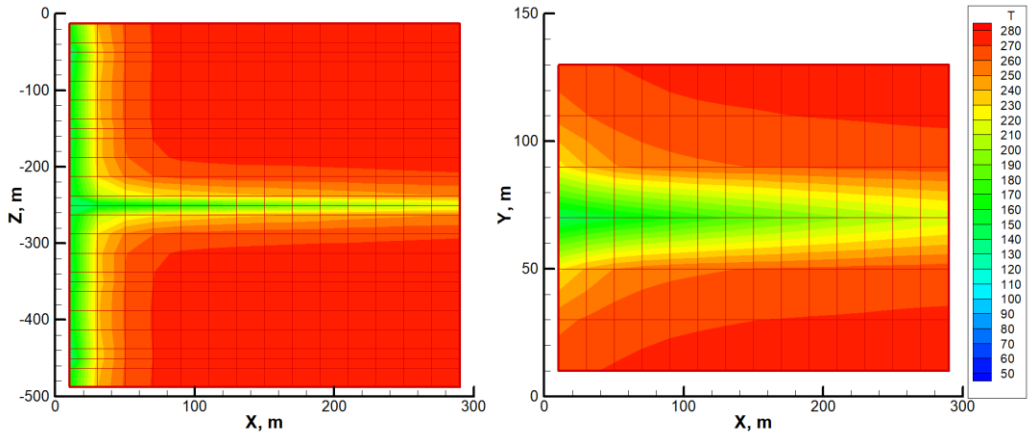

Figure 19: Temperature profiles in EGS after twenty years of water injection.

Finally, we considered a hypothetical PPG treatment after ten years of water injection where the highly conducting fracture would be blocked by PPG and simulated that case until twenty years. The temperature profiles for this case are shown in Figure 20.

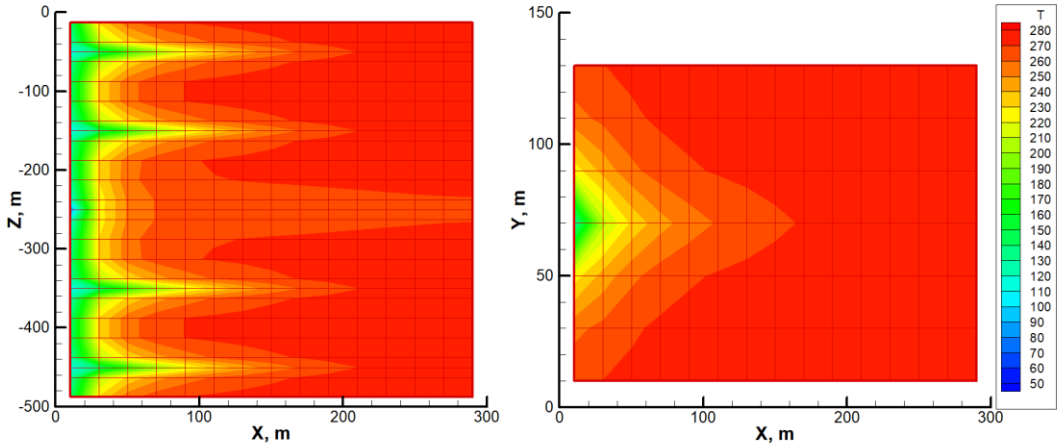

Figure 20: Temperature profiles in EGS after twenty years of water injection with PPG blocking the middle, highly conducting fracture after ten years.

Injected water only flows through the other four fractures. The xz-cross section on the left shows thermal depletion around those fractures. In addition, heat has flown to the region around the highly conducting fracture. The xy-cross section on the right shows thermal depletion around one those fractures, whose extent is much less than that for the highly conducting fracture at ten years in Figure 18, since that fracture had a quarter of the flow the highly conducting one had.

After ten years of water injection, $1.63 \cdot 10^{14}$ J of energy were produced. For another ten years of water injection with no PPG treatment, an additional $1.46 \cdot 10^{14}$ J of energy were produced, which was less than that for the first ten years. For another ten years of water injection with PPG treatment, an additional $1.78 \cdot 10^{14}$ J of energy were produced, which is 22% more than without PPG treatment.

5. SUMMARY AND CONCLUSIONS

We developed a mathematical model and numerical simulator to simulate PPG injection into EGSs in order to divert flow from highly conductive fractures to less conductive ones. The starting point for our mathematical model is the TOUGH2-CSM multiphase, multi-component, and multi-porosity formulation. We modified that formulation to simulate injection of PPG into fractures. We developed an equation of state module for gel-water systems based on a module that handles air and water since PPGs consist mostly of water. We use experimental studies of PPG flow through fractures to obtain the PPG flow formulation as well as formulations of longitudinal and transverse dehydration. In addition, we added the ability of PPG to swell over time.

Our simulator's features were verified by matching data from experimental studies. They include PPG injection into open fractures, which were used to verify our PPG rheology and longitudinal dehydration models, and PPG injection into a closed fracture, which were used to verify our transverse dehydration model. Finally, we applied our model to a synthetic EGS to ascertain the effect of blocking highly

conductive fractures with PPG on energy production and found significantly more energy can be produced. Our model performed well on the above cases and we will be applying it more extensively to modeling PPG injection into EGSs in the future.

6. ACKNOWLEDGEMENTS

This material is based upon work supported by the U.S. Department of Energy's Office of Energy Efficiency and Renewable Energy (EERE) under the Geothermal Technologies Office (GTO) INNOVATIVE METHODS TO CONTROL HYDRAULIC PROPERTIES OF ENHANCED GEOTHERMAL SYSTEMS Award Number DE-EE0009790. This work is also supported by EMG Research Center in Colorado School of Mines.

7. REFERENCES

Bai, B., 2023a. PPG Retention and Dehydration in Fractured Carbonates, to be published.

Bai, B., 2023b. Quarterly Research Performance Progress Report for DE-EE0009790, Innovative Particle Gels for Controlling Preferential Fluid Flow in Geothermal Reservoirs to Enhance Heat Recovery, Oct 1, 2023 to Dec 31, 2023.

Bai, B., Li, L., Liu, Y., Liu, H., Wang, Z., and You, C. 2007a. Preformed Particle Gel for Conformance Control: Factors Affecting its Properties and Applications. SPE Reservoir Evaluation and Engineering 10 (4): 415-421. SPE-89389-PA.

Bai, B., Liu, Y., and Coste, J.-P. 2007b. Preformed Particle Gel for Conformance Control: Transport Mechanism through Porous Media. SPE Reservoir Evaluation and Engineering 10 (2): 176-184. SPE-89468-PA. Doi: 10.2118/89468-PA.

Charoenwongsa, S. , Kazemi, H., Fakcharoenphol, P., and J. L. Miskimins, 2012. Simulation of Gel Filter Cake Formation, Gel Cleanup, and Post-Frac Well Performance in Hydraulically Fractured Gas Wells. Paper presented at the SPE International Symposium and Exhibition on Formation Damage Control, Lafayette, Louisiana, USA, February 2012.

Goudarzi, A., Zhang, H., Varavei, A., Hu, Y., Delshad, M., Bai, B., and Sepehrnoori, K., 2013. Water Management in Mature Oil Fields using Preformed Particle Gels,Paper SPE 165356, presented at the SPE Western Regional & AAPG Pacific Section Meeting, Monterey, California, April, 19-25.

Habanero Geothermal Project Field Development Plan, 2014. Document Number: COM-FN-OT-PLN-01166, Date: 9 October 2014, Geodynamics, Ltd.

Howard, G.C. and Fast, C.R.: Optimum Fluid Characteristics for Fracture Extension," Drilling and Production Practices, API (1957) 261.

J.W. Lund, Characteristics, development and utilization of geothermal resources, Geo-Heat Cent Q Bull 28 (2) (2007) 1–9.

Narashimhan, T. N. and P. A. Witherspoon. 1976. An integrated finite difference method for analysis of fluid flow in porous media. Water Resources Res. 12: 57–64.

Pruess, K., and T. N. Narasimhan, 1985. A Practical Method for Modeling Fluid and Heat Flow in Fractured Porous Media, Soc. Pet. Eng. J., 25, pp. 14-26.

Pruess, K., C. Oldenburg, and G. Moridis. 1999. TOUGH2 User's Guide, Version 2.0. Report LBNL-43134, Lawrence Berkeley National Laboratory, Berkeley, California.

Seright, R.S. 2001. Gel Propagation through Fractures. SPE production & facilities 16(4): 225-231. SPE –PA. DOI: 10.2118/74602-PA

Seright, R. S. "An Alternative View of Filter-Cake Formation in Fractures Inspired by Cr(III)-Acetate-HPAM Gel Extrusion." SPE Prod & Fac 18 (2003): 65–72.

Wang, Z., and Bai B, 2018. Preformed-particle-gel placement and plugging performance in fractures with tips. SPE J 2018. https://doi.org/10.2118/193997-PA.

Warren, J.E. and Root, P.J., 1963. The Behavior of Naturally Fractured Reservoirs. Society of Petroleum Engineers Journal, Transactions AIME, 228, September 1963, pp. 245-255.

Winterfeld P. H. and Y.-S. Wu. 2014. Simulation of CO2 sequestration in brine aquifers with geomechanical coupling. In Computational Models for CO2 Sequestration and Compressed Air Energy Storage, edited by J. Bundschuh and R. Al-Khoury, New York, NY, CRC Press.

Winterfeld, P. H. and Y.-S. Wu. 2016. Simulation of Coupled Thermal/Hydrological/Mechanical Phenomena in Porous Media. SPE Journal 21 (3): 1041–49.

Winterfeld, P. H., B. Johnston, K. Beckers, and Y.-S. Wu. 2019. Reservoir simulation code for modeling chemical tracers and embedded natural fractures at EGS Collab, presented at 44th Workshop on Geothermal Reservoir Engineering, Stanford University, Stanford, California, February 11-13.

World Energy Balances: Overview, IEA, Paris https://www.iea.org/reports/world-energy-balances-overview, Licence: CC BY 4.0

Wu, Yu-Shu, and Karsten Pruess, 1988. A Multiple-Porosity Method for Simulation of Naturally Fractured Petroleum Reservoirs. SPE Res Eng 3 (1988): 327–336.

Zhang, H., and Bai, B. 2010. Preformed Particle Gel Transport through Open Fracture and its Effect on Water Flow. SPE Journal 16(2): 388-400. SPE-129908-PA. DOI: 10.2118/129908-PA

Zhang, Keni., Yu-Shu Wu, and Karsten Pruess, "User's Guide for TOUGH2-MP - A Massively Parallel Version of the TOUGH2 Code," LBNL-315E, Earth Sciences Division, Lawrence Berkeley National Laboratory, May, 2008